Geomorphology 449 (2024) 109065

Contents lists available at ScienceDirect

Geomorphology

journal homepage: www.journals.elsevier.com/geomorphology

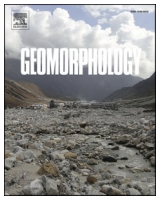

# A cost-effective image-based system for 3D geomorphic monitoring: An application to rockfalls

Xabier Blanch [a,b,*], Marta Guinau [a], Anette Eltner [b], Antonio Abellan [c]

[a] RISKNAT Research Group, GEOMODELS Research Institute, Universitat de Barcelona, 08028 Barcelona, Spain
[b] Institute of Photogrammetry and Remote Sensing, Technische Universität Dresden, 01062 Dresden, Germany
[c] Center for Research on the Alpine Environment (CREALP), Sion, CH1950, Valais, Switzerland

ARTICLE INFO

*Keywords:*
Photogrammetry
Rockfalls
Structure-from-motion
Natural hazard

ABSTRACT

Change-detection monitoring plays a crucial role in geoscience, facilitating the examination of earth surface processes and the mitigation of potential risks due to natural hazards. A significant aspect of this monitoring involves the use of images, enabling 2D to 4D monitoring approaches. Our objective is to bridge the knowledge gap in developing very low-cost camera units by providing insights into specific products, assembly processes, and utilized codes. The presented approach involves prioritizing cost reduction albeit a trade-off in system quality. The results obtained in the study area of Puigcercós cliff in Spain demonstrates the system's efficacy in detecting rockfalls and pre-failure deformation with a notable level of detection of only 8 cm in the change detection analysis. Additionally, two system versions are presented; one emphasizing real-time image transmission, while the other provides a simpler, energy-efficient approach conducive to long-term data capture using a single battery. Both solutions showcase the potential of leveraging very low-cost technology in geohazard monitoring.

## 1. Introduction

The utilization of remote sensing techniques, specifically optical imaging sensors, for the observation and monitoring of natural processes in the geosciences has become a widely accepted strategy (Leprince et al., 2008; Scaioni et al., 2014; Eltner et al., 2016). This approach allows for direct observation of the natural environment, enabling the study of the evolution of geomorphology processes. Recent technological advances have greatly simplified the capture high-quality images and optical sensor technology has made significant progress with the mass production of CMOS sensors, which are widely used in consumer digital cameras and smartphones (Toth and Jóźków, 2016). Recent advancements in computer vision algorithms coupled with the ability to obtain images from novel platforms such as uncrewed aerial vehicles (UAVs) and shipborne (Colomina and Molina, 2014; Jin et al., 2021) are driving significant advances in different fields of geoscience and geomorphology discipline (Giordan et al., 2022), as evidenced by several examples spanning a wide variety of disciplines such as: a) the ability to automatically calculate the volume of material eroded in gullies (Kaiser et al., 2014; Stöcker et al., 2015; Neugirg et al., 2016); b) the development of tools to monitor rivers using images and videos (Eltner et al., 2021); c) the advances in the multitemporal monitoring of rockfalls (Kromer et al., 2019; Blanch et al., 2021) or coastal erosion (Gonçalves and Henriques, 2015); d) the study of glacier dynamics (Rivera et al., 2012; Taylor et al., 2021) and associated tsunami waves (Minowa et al., 2018) and e) the continuous monitoring of volcano systems using infrared cameras (Spampinato et al., 2011; Patrick et al., 2014).

Recent technological advances have resulted in the emergence of cameras with improved sensor quality, larger sensor sizes and higher number of megapixels on the market. It is now possible to acquire digital single-lens reflex cameras (DSLR) with >45 megapixels (MPx), drones with high-quality cameras or smartphones with photographic sensors, and these advancements have helped to democratise and expand the possibility of capturing images. In contrast to those advancements, there has also been the emergence of very low-cost cameras like wild cameras or single board camera systems that are capable of capturing images and videos efficiently, albeit at a lower quality. For instance, very low-cost cameras such the Raspberry Pi Camera V2 (25€) from the Raspberry Pi foundation have become increasingly popular for deployment in remote study areas because of their simplicity of use, cost efficiency and low power consumption (Pagnutti et al., 2017; Eltner et al., 2018; Taylor et al., 2023). Such very low-cost require only basic programming skills

* Corresponding author at: Institute of Photogrammetry and Remote Sensing, Technische Universität Dresden, 01062 Dresden, Germany.
*E-mail address:* xabier.blanch@tu-dresden.de (X. Blanch).

https://doi.org/10.1016/j.geomorph.2024.109065
Received 30 May 2023; Received in revised form 9 January 2024; Accepted 9 January 2024
Available online 15 January 2024

to capture data, as they typically do not need to be integrated with other complex systems. The flexibility and simplicity of use of these systems may result in more reliable systems, in contrast to solutions that rely on different hardware and complex solutions for integration. These systems have a wide field of application in the monitoring of natural processes, both in two-dimensional (2D) environments when using a single camera and in three-dimensional (3D) scenarios when using an array of cameras.

Images captured by Raspberry Pi Cameras are primarily utilized for 2D monitoring nowadays (Wilkinson et al., 2021), but they can also be used for advanced 3D monitoring through the application of Structure-From-Motion with Multi-View Stereo (SfM-MVS) photogrammetry techniques. The application of 3D monitoring has been recently applied across different environmental contexts, further emphasizing its potential as a cost-effective and versatile solution. Some examples include: a) the monitoring of rockfalls (Blanch et al., 2020); b) the experimental system to study the stability in open-pit highwalls (Santise et al., 2017), c) the 3D modelling capabilities from a low-cost system mounted on a UAV (Piras et al., 2017) and d) the recent work by Taylor et al. (2023) on 3D monitoring of glacier calving using Raspberry Pi cameras.

### 1.1. Structure from motion and low-cost monitoring systems

SfM-MVS is a well stablished procedure in the field of photogrammetry, with its fundamental principles fully described in previous publications (Westoby et al., 2012; James and Robson, 2014; Iglhaut et al., 2019; Eltner and Sofia, 2020). The overall concept of this technique relies on estimating point coordinates in the 3D object space using their corresponding 2D points in the image space. One of the advantages of this technique is the ability to use almost any image source (ease of data acquisition) and the ability to automate the entire 3D reconstruction process (processing large amounts of data). In contrast to the large costs associated with traditional Light Detection and Ranging (LiDAR) point cloud data collection methods, the emergence of low-cost 3D monitoring techniques has provided a more democratized access to data acquisition, enabling the study of a wider range of natural environments with increased spatiotemporal frequency (Anderson et al., 2019).

The generation of 3D models using SfM-MVS algorithms typically involves capturing several images of the same surface from different perspectives using a single or multiple cameras moving around the object using well-stablished structure from motion procedures. However, this approach might not be optimal for geoscientific monitoring because repeated site surveys are needed to study the dynamics of environmental process (Taylor et al., 2023). To address the need for investigating active processes in geoscientific monitoring, the installation of an array of fixed time-lapse camera systems in the study area can provide a more frequent 3D and fully autonomous model generation than “one shot” fieldwork campaign. The use of these systems also allows for the use of advanced post-processing techniques to increase the quality of the point cloud comparison by leveraging the invariable position of the cameras (Santise et al., 2017; Feurer and Vinatier, 2018; Blanch et al., 2021).

In regard to financial considerations, it should be noted that within the literature, the term “low-cost photogrammetric monitoring system” is generally associated to the use of DSLR cameras and drones (Anderson et al., 2019). However, the use of alternative cameras such as the Raspberry Pi Camera systems typically costing only tens of euros would need to be considered as “very low-cost systems” in comparison to the normal price of a standard consumer camera or a UAV acquisition system, which can cost thousands of euros making them difficult to implement in disadvantaged economic contexts.

While multiple experiences of photogrammetric systems using DSLR cameras can be found in the literature (Roncella et al., 2014; Eltner et al., 2017; Kromer et al., 2019; Brezzi et al., 2020; Giacomini et al., 2020). There are a limited number of publications discussing the use of fixed systems designed with a cost-minimisation objective (Santise et al., 2017; Taylor et al., 2023). The closest experience to the present study is the preliminary test conducted by Santise et al. (2017) in the Pilkington Street Reserve, Australia. These authors employed five Raspberry Pi cameras on a small rock face, aiming to evaluate the adequacy of this very low-cost system for monitoring purposes. More recently, Taylor et al. (2023) also explored the potential of using images from a Raspberry Pi camera to perform 3D monitoring from different perspectives. Their work explores the usability of very low-cost cameras for glacial monitoring, comparing the results obtained with UAV systems and providing a valuable application example. Despite the growing interest in those systems, to the best of our knowledge, there have been no attempts to openly share the design details and necessary codes to operate them in a fixed, remote and multi-camera mode. The occasional absence of an open policy could make it difficult for other researchers to replicate and improve on previous research; therefore, we offer technical development of our systems and the corresponding codes.

The authors have previously published photogrammetry systems that use high-resolution DSLR cameras (> 40 MPx) to monitor rockfalls in near real time (Blanch et al., 2023). In contrast, in this work, both the methodology and the results are focused on significant cost reduction and simplification of the implementation and working codes, making them accessible to the community lacking this type of knowledge. Thus, the system introduced in this study, is less complex, requires fewer economic resources and knowledge for their correct implementation. The authors' aim in applying both systems to the same study area and to the same natural process to facilitate the comparability of the results, highlighting both the similarities (the concept) and differences between the systems (e.g., ease of assembly and level of detection (LoD)), and ultimately, as Taylor et al. (2023) and Santise et al. (2017) have shown in the past, demonstrate that very low-cost photogrammetric monitoring of geomorphological processes is feasible.

Therefore, this manuscript presents a comprehensive examination of the essential specifications and requirements for the conceptualization, design, and operation of autonomous systems, eliminating the need to change batteries, extract the images and configure the system in the field. These systems are developed from two different points of view, one is more complex as it includes real-time image transmission, and consequently a more complex configuration, requiring more infrastructure and higher power consumption, and the other is simpler, storing the images on a USB stick, and optimised for reduced power consumption and ease of installation. An in-depth description of the various components and their assembly is provided with a focus on real-world applications in need of reliable systems for diverse geo-hazard monitoring applications. Our study covers the discussion of technical, ensemble and environmental constrains and possible solutions aiming to facilitate replication in other scenarios. We offer a detailed analysis of the systems, along with a real application case and its results, aiming to guide researchers without extensive expertise in photography, electronics, or computer science on setting up a very low-cost monitoring system capable of capturing valuable data for geoscience monitoring. Authors advocate for the open dissemination of knowledge to increase our understanding of natural processes by facilitating the acquisition and treatment of 3D data regardless of economic constraints.

## 2. Material and methods

### 2.1. Photogrammetric systems

The defining characteristics of photogrammetric systems are diverse in the literature. The systems we have developed in this publication meet the requirements outlined in Blanch et al. (2023), as they are fixed time-lapse systems that are designed to capture images on demand, automatically transfer them to a server and are power autonomous systems. However, the photographic acquisition units described in this publication can also be installed individually for 2D monitoring. The simplified version of the system does not fit the description of a photogrammetric system defined in Blanch et al. (2023), as it does not

allow real-time monitoring, nor does it have solar panels, but its ease of installation and set-up, together with its low power consumption and very low cost, can make it a very useful tool for geomorphological monitoring where data collection is not a problem, or for remote areas where data transmission is impossible. Finally, the proposed modular design allows alternating between the different versions proposed, so that each new system can be adapted to the specific needs of each investigation.

### 2.2. Components of the photogrammetric systems

This section provides a brief explanation of the components and technical specifications necessary to assemble the photogrammetric systems. The system's main characteristics are tailored to a specific case study involving rockfall detection in a cliff in Puigcercós, Spain (Fig. 1a). Authors of this manuscript share full details of utilized brands and models to facilitate replicability by non-experts in different fields of knowledge. While other multiple options are available on the market - some of them are listed in the discussion section. -, the use of similar components as those listed here below will facilitate software compatibility. Furthermore, open code policy is intended to facilitate quick installation and user-friendly operation - plug&play - with the proposed hardware.

#### 2.2.1. Image sensor and lens

The sensor and the lens form the core of the image acquisition, being key elements both in terms of quality and cost. Five very low-cost photographic modules were installed in the Puigcercós study area. Each photographic module is composed of a Sony IMX219PQ back illuminating image sensor of eight megapixels (a detailed review of this component can be found at Pagnutti et al. (2017)), mounted on a commercial Raspberry Pi Camera Module V2 board (Fig. 1a). This sensor comes with a stock 3.04 mm focal length plastic lens (equivalent to 29 mm in 35 mm format) and a maximum aperture of f/2.0. While this combination of sensor and lens are highly cost-efficient, it also suffers from limitations (Bowman et al., 2019; Elias et al., 2020) that are mainly in terms of image quality (Luhmann et al., 2016) and can affect the final 3D models, in terms of geometric quality and level of detail.

#### 2.2.2. Control unit and real time clock

The control unit (Fig. S1b) and Real Time Clock (RTC) (Fig. 1c) manage camera settings and triggering process. The control unit is based on the commercial minicomputer boards (SBc) Raspberry Pi (Fig. 1bc), which are small single board computers produced by the Raspberry Pi Foundation (Cambridge, United Kingdom). Due to the low-cost of the single-board computer, the simplicity of the system and its great flexibility, this microcomputer is widely used in the scientific community, especially in the field of natural sciences and image processing (Jolles, 2021; Kishan et al., 2022; Vedavalli et al., 2022). All Raspberry Pi models are useful for the development of systems, which are also undemanding in terms of computational power. From the top-of-the-range boards with higher computing power and consumption (Raspberry Pi 4) to those with a small form factor and low power requiriments (Raspberry Pi Zero), they are all suitable for image acquisition. Details such as integrated WiFi or the need to solder pinouts for the small form factor boards should be taken into account.

Raspberry Pi systems lack an internal battery, so they are unable to save the current time and date. To overcome this limitation, a UUGear WittyPi shield board (Fig. S1c) was used in this research as RTC to attempt to synchronize camera triggering. This proposed board can also manage power supply, for instance by turning on the system or shutting it down on demand. The combination of these two properties allows the WittyPi to be used for scheduling by defining complex ON/OFF Raspberry PI sequences (UUGear WittyPi3, 2021).

#### 2.2.3. Network communication system

Data transmission and connectivity (Fig. S1d) was guaranteed using mobile phone data network (4G). To link the 4G mobile signal to the photogrammetric systems, a wireless network was designed. The proposed system used the 2.4 GHz Wi-Fi frequency, which allows greater distances to be reached, although it does not provide as much speed as 5.0 GHz networks. A more detailed description of the transmission module is addressed in Blanch et al. (2023) of this study.

Providing connectivity to the photographic modules is a key-point to control the setup but it is not sufficient to transfer images remotely. Thus, for this specific development, the commercial Dropbox service was used to transmit the images directly from the control unit to the server. This solution was used for two reasons, namely: the possibility to

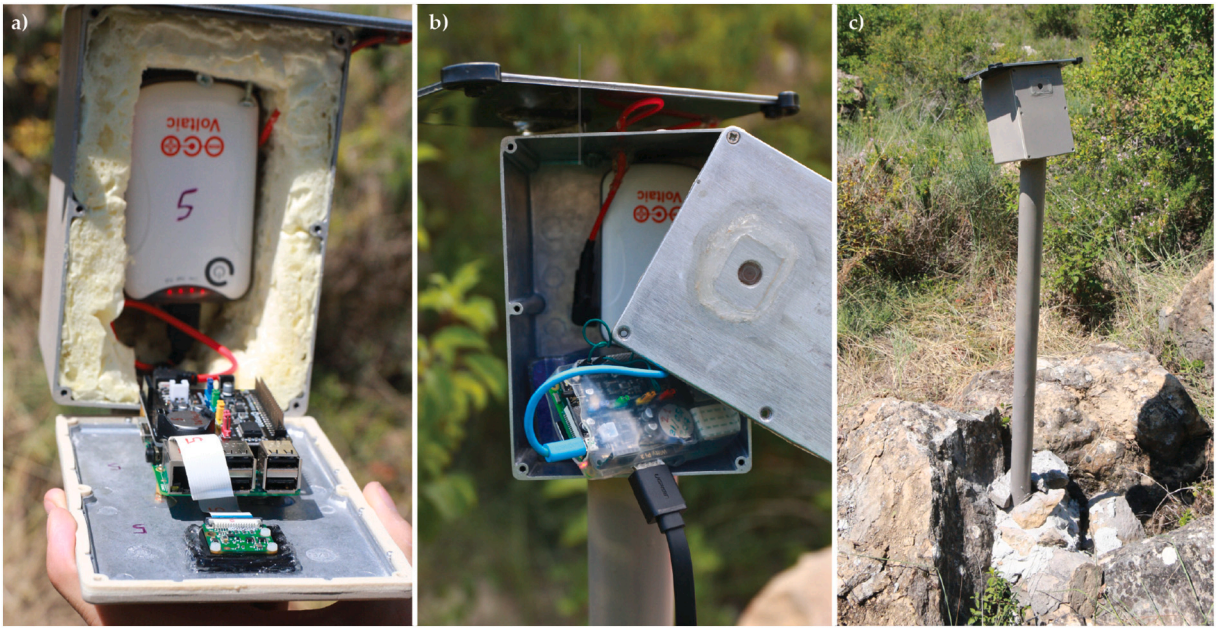


**Fig. 1.** Images of the photogrammetric systems installed in the study area. a) General image of a system showing the support made from concrete-filled pipe. b) Image showing the metal box and the hole for the lens covered with laboratory glass. c) Image showing the inside of the device with the connections shown in Fig. 3.

interact with Python scripts regardless of the operating system, and the non-complex integration into the end servers with a smooth learning curve for day-to-day usage. Other options for automatically transmitting data to the server include secure file transfer protocol (SFTP) solutions for own servers, as well as other client-server software for file hosting services (e.g., GDrive, OneDrive), some of them open source (e.g., Nextcloud).

#### 2.2.4. Power supply components

The proposed very low-cost systems use a 5 V power bank (Fig. S1e and 1bc) to supply power, which is charged by a 3.5 W solar panel (Fig. S1f) at each module. Importantly, the power bank shall be able to function on a so-called *Pass Through Charging* technology to supply energy to the photogrammetric system while the power bank is being charged. Due consideration on this aspect is needed because most power banks do not allow charging simultaneously to power receiving. It should also be noted, for severe climate environments, the safety limitations associated with temperatures. In the case of the power banks used, the input (solar charging) operates within a range of 0 °C to 45 °C, and the output (providing power to the system) has a wider range from −15 °C to 60 °C. Due the difficulty to work with a specific power bank, this research also addresses other more accessible options. For example, another option it is the usage of 3.7 V lithium batteries (Fig. S1e). These batteries, whose name depends on their physical dimensions (e.g., 18,650 or 18,500), can contain between 1400mAh and 3500mAh. Use Li-Ion cells increases the complexity of the system, as the plug and play concept of the aforementioned components is lost (the lithium cell needs a Battery Management System (BMS) and a solar charge regulator). However, it can be a suitable low-cost alternative in the face of difficulties in supplying specific solar powered power banks.

Lithium batteries can be used individually for 3.7 V or they can be stacked. Depending on how they are stacked, in series (S) or in parallel (P), higher voltage or higher capacity batteries are obtained. Packs stacked in parallel allow higher capacity (e.g., 1S2P means 2 cells in parallel, doubling the capacity but maintaining the voltage). Alternatively, cells can be added in series to achieve higher voltages for the same capacity (e.g., 2S1P provides 7.4 V). A combination of both stacking strategies is also possible (e.g., 2S2P is a 4-cell battery with double the voltage and capacity of a single cell). In all cases, the voltage must be changed to 5 V, as this is the Raspberry Pi's nominal voltage. This step-down or step-up operation must be done using external components. In the case of step-down (batteries with a voltage higher than 5 V), this can be done directly on the WittyPi, saving the need for additional components.

#### 2.2.5. Protective case

All components (except for the solar panel) must be integrated into a waterproof container (Fig. 1a) to isolate the electric components from dust, rain, and snow. Two holes were drilled in the box utilized in this study. One hole was drilled to place a window for the camera, which was then protected with laboratory glass and insulating silicone. And the second hole was drilled to introduce the cable from the solar panel to the power bank (Fig. 1b). The camera is mounted to the box using small plates specifically designed for the Pi Camera V2 (Fig. 1a). Since the box is made of metal, special consideration is needed to ensure that no electrical components are in contact with the surface of the box (Fig. 1ab).

The cost of the proposed system may vary slightly depending on the capacity of the powerbank, the solar panel required, and the Raspberry Pi model used, as well as the availability of these items in scarce contexts. The Raspberry Pi, together with the Pi Camera V2 and Witty Pi components, could cost between 65€ for the Raspberry Pi Zero W and 85€ for the Raspberry Pi 3 model. The powerbank and solar panel cost approximately 70€, although this can vary greatly depending on the capacities required. Additional costs, such as casing, glass and fixing the system, as well as other additional accessories, can realistically amount to 80€. Consequently, the total estimated cost for the installation of this system is around 225€-250€ per camera.

### 2.3. Module assembly

One advantage of using a system based on the Raspberry Pi board is the simplicity of assembly, as the camera module, microcomputer and RTC board are all part of the same "ecosystem". The connections (also described in the respective manuals and linked under extra content) must be made as follows (Fig. 2). In order to connect the camera module, the flat ribbon cable needs to be connected to the specific camera port on the Raspberry Pi (extra content). Subsequently, the WittyPi board is connected to the top of the Raspberry Pi using the 2 × 20 pin header (extra content).

The power bank is connected via a USB cable directly to the WittyPi board (Fig. 2). In case of solar panel usage, the panel is connected to the battery via the corresponding port at the power bank (in most cases, a USB socket) (Fig. 2). The solar panel can be placed flat on the box. However, considering small angle brackets allows the solar panel to be installed in an inclined position depending on the latitude at which the system is setup to improve the solar energy collection efficiency. If lithium batteries are used (Fig. 2), a BMS (discharge protector) or a Li-Ion charger (including BMS) must be mounted at the input to protect the cells from over and undercharging. In addition, a voltage conversion is required at the output. In that case it is important to ensure that the additional equipment (BMS, DC-DC converter) is appropriate in terms of both current and voltage. The use of different versions of this hardware can simplify the use of components. For example, new versions of WittyPi Mini can be connected directly to 3.7 V Li-Ion cells (supplementary material). Further details on assembling the individual hardware components can be found in the respective manuals as well as in the datasheets of all electronic components.

### 2.4. Proposed workflow and software

This section describes in detail the specific workflow developed to capture images, logs and to perform remote data transfer (Fig. 3). While specific details are publicly shared in the author's repository (https://github.com/xabierblanch/RasPi-System), a complementary description of the installation of the operating system (OS) and basic software required for the correct implementation of the systems are available in the supplementary material.

Fig. 3 illustrate the proposed workflow where the photographic modules are programmed to run a pipeline that: i) starts with the photo acquisition, ii) followed by renaming the image to the acquisition date and time, and iii) then, the file is stored in a temporal folder on the control unit. After these steps of the workflow two modes of operation follow. If the device has an internet connection, iv) the images are uploaded directly to the server and then v) stored in a backup folder for 15 days in the control unit. If there is no internet connection, the images remain in the temporal folder and the device will continue capturing images until the memory is full. As soon as there is an internet connection, the images are transferred to the server and then deleted from the temporal folder. The codes are divided into main and auxiliary codes written in Python and bash programming languages. Fig. S2 shows the structured flow chart of all the operational codes shared in the repository.

The main code (*main.py*) is in charge of performing the following operations (Fig. S2):

1. Create/check correct paths
2. Set capture properties (ISO, resolution, meter mode…)
3. Remove old files (more than X days) from "backup folder"
4. Take (library: *PiCamera*) and save (datetime format) pictures
5. Store it in "temporal folder"
6. Try to upload to Dropbox server (library: *Dropbox*)

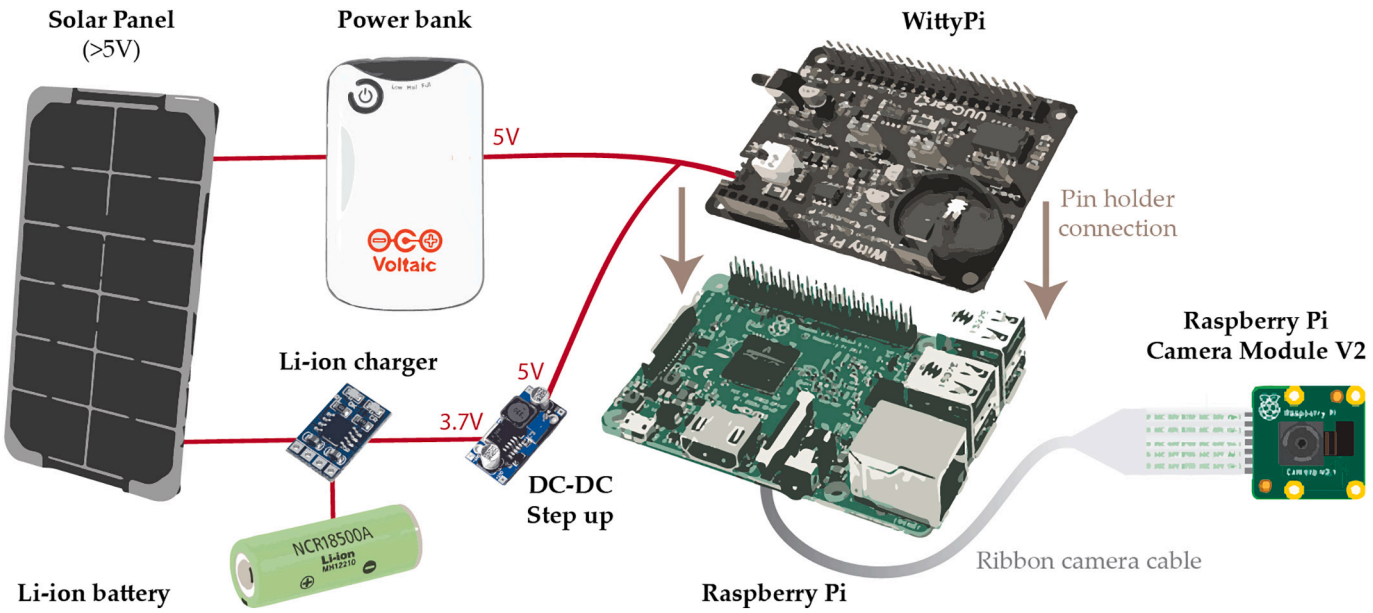


**Fig. 2.** Sketch of the component's assembly. The camera is connected to the Raspberry Pi using the ribbon camera cable. The RTC is connected to the control unit by means of the pin holder connection. The solar panel and the power bank are connected to the WittyPi via cable or USB. The power bank can be replaced by the lithium cell in combination with the DC-DC converter.

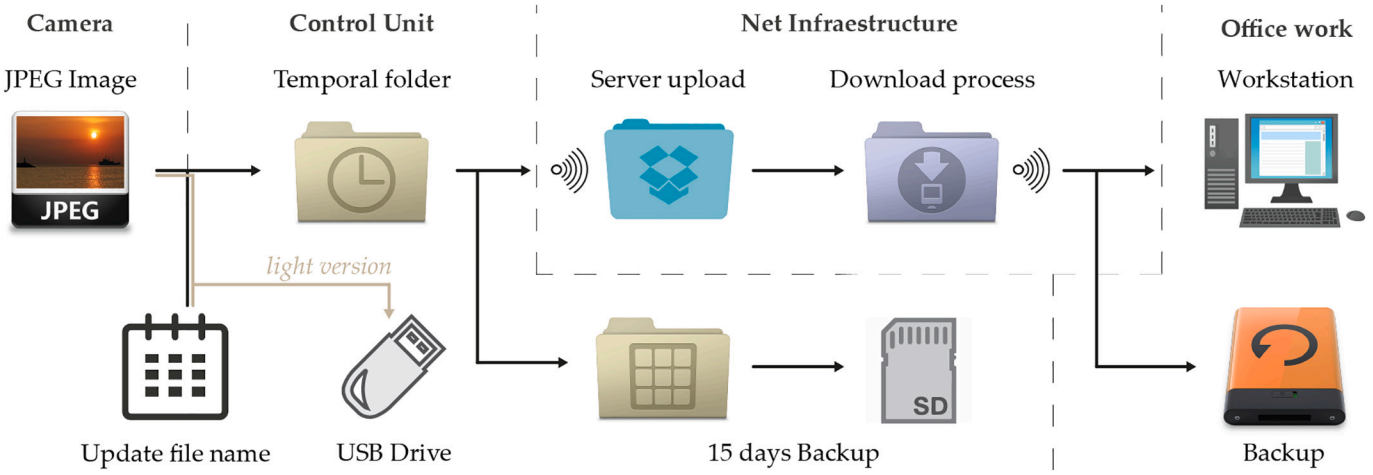


**Fig. 3.** Illustrative scheme of the workflow implemented in the control unit to send the images remotely, avoiding filling the internal memory of the devices. The light version only stores the images in the USB drive.

a. If success - > Move to backup folder
b. If fails - > remain in "waiting net folder"

The "main.py" script saves the text output to a log file to monitor the operation of the device on each run and to provide more information in the event of system failures. This text file is stored in a specified folder. The log files automatically generated by the WittyPi are also copied to this folder.

Finally, the "logs.py" code uploads all these log files to the corresponding server, thus allowing the control and logging of the device's operation as long as the connection is available. To run the codes automatically on system start-up, the crontab application (Linux operating system) is used to run a bash code called "run.sh". This code performs the basic tasks of generating the appropriate paths, running the Python codes and finally shutting down the system by activating the WittyPi hardware.

There is also a simplified version of the code that solely stores the images on an external USB flash drive connected to the Raspberry Pi and does not send remote images (Fig. 4). This configuration cannot be considered as a real-time photogrammetric monitoring system. However, it simplifies the installation because it does not require any communication system, reduces energy consumption (ideal for use with Li-Ion cells) and simplifies the code and the use of external libraries (less chance of being deprecated). In addition, a ready-to-use image file with the light versioning system is distributed in the author's repository. (Appendix B includes a link to the .ISO image). More information about the installation of the ready-to-use image file is provided in the Supplementary Material.

## 3. Results

### 3.1. Implementation in a real scenario

The proposed photogrammetric system has been deployed in an area with high rockfall activity: the Puigcercós cliff (Catalonia, Spain), with an experimental setup running for more than two years (Blanch, 2022).

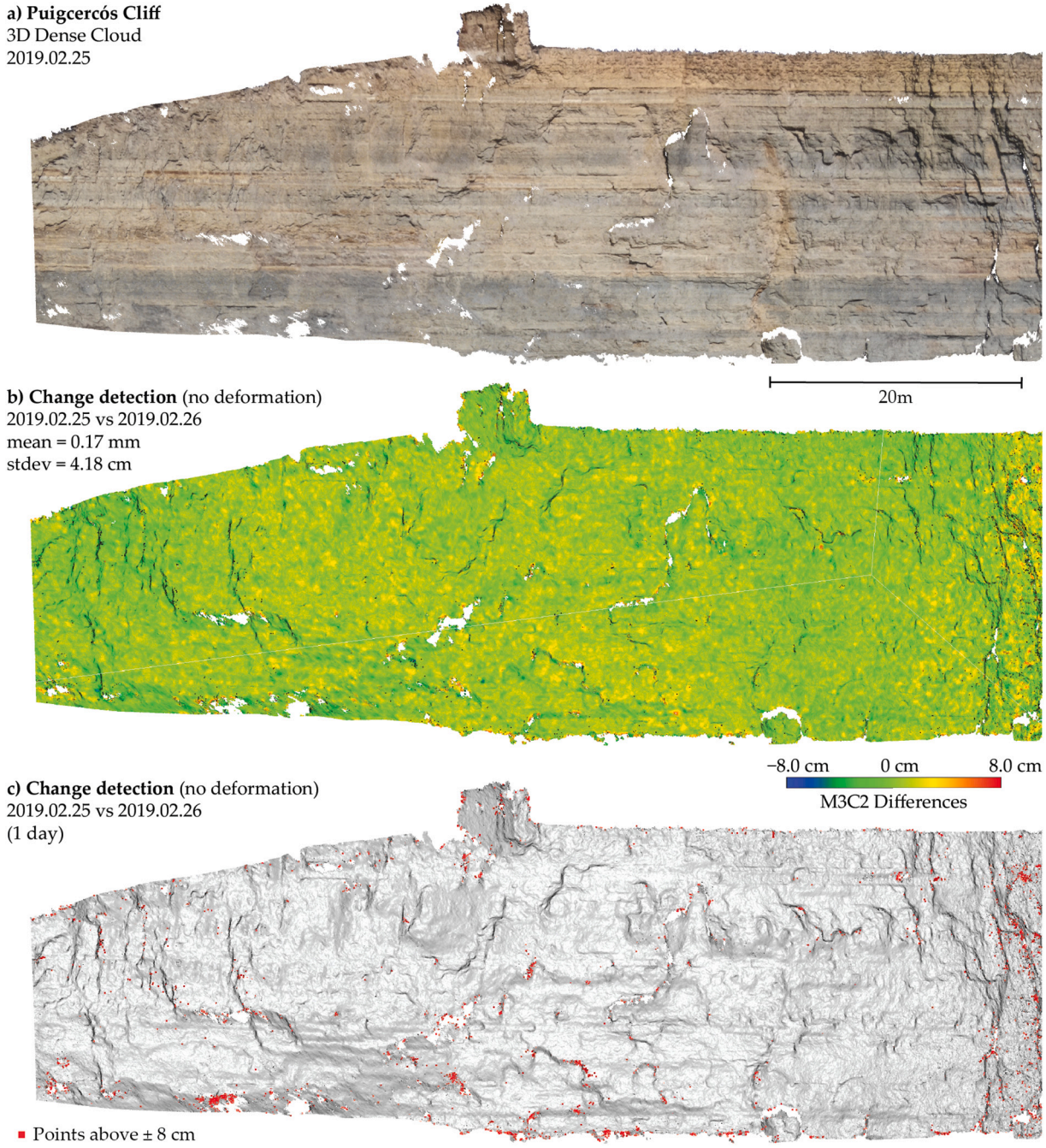


**Fig. 4.** a) Point cloud obtained with the very low-cost photogrammetric system installed in Puigcercós (obtained with MEMI workflow). b) M3C2 comparison of two consecutive days (no expected deformation). c) In red, points with a deformation greater than ±8 cm (theorical detection threshold). (For interpretation of the references to colour in this figure legend, the reader is referred to the web version of this article.)

Five very low-cost photogrammetric systems were installed, consisting of photographic and data transmission modules. The cameras were installed at 70 m distance to the escarpment and at a distance between cameras (i.e., base) of about 20 m. All of them are installed at the same height above the ground (1.5 m), and the difference in height between them is no more than half a meter. Each camera captured the entire central part of the escarpment yielding an almost complete overlap between images. This distribution, in conjunction with the properties of the Pi Camera V2, results in a ground sample distance (GSD) of 2.8 cm per pixel. Fig. S3 in the supplementary material shows an image of the cliff obtained from each camera. The system was configured to capture a burst of 15 images once per day to improve the photogrammetric models. The cameras were operational from July 2018 to February 2020, with at least 4 out of 5 cameras in operation throughout the study period. On 9 days, only 3 cameras were operational. However, this was sufficient to complete the photogrammetric reconstructions. This was carried out through different advanced techniques such as point cloud stacking (PCStacking) and multi-epoch multi-imagery (MEMI) that are thoughtfully described in Blanch et al. (2020 and 2021). The system enabled investigating rockfall activity using M3C2 change detection algorithms (Lague et al., 2013) applied to 3D models. Fig. 4a shows a 3D model of the Puigcercós cliff obtained with this photogrammetric system and using the MEMI workflow (Appendix A includes a link to a viewer to visualize the 3D model). Using the MEMI workflow (Blanch et al., 2021) and the Agisoft Metashape software with the highest-quality settings, we obtained a dense point cloud of roughly 3.3 million points after filtering

and clipping the scarp. The average point surface density is 1666 points/$m^2$, which is 72 % lower than the densities reported in Blanch et al. (2023). The RMS reprojection error for the camera estimation in both epochs is 0.41 pixels.

The 3D models were scaled with virtual Ground Control Points (GCPs), which were extracted from a terrestrial LiDAR model of the same study area. This strategy involves extracting the 3D coordinates of hand-selected features from the scaled LiDAR model that are manually linked to 2D pixels of a reference image. To maintain correspondence over the time series of images the MEMI workflow uses a Lucas–Kanade algorithm to track these selected pixels in subsequent images, ensuring that all change detection processes have a true scale.

The proposed system acquired images with suboptimal quality, resulting in photogrammetric models with relatively low level of detail (Fig. 4a). Nevertheless, recurrent imaging (burst mode) and enhancement strategies allowed the generation of models with acceptable level of detection in change detection analysis (Fig. 4b). Following the estimation of change detection thresholds established by Abellán et al. (2009) for LiDAR datasets, we estimate the LoD of our photogrammetric system by comparing two 3D models generated on consecutive days during a period of no observable rockfall activity. While the expected change should be zero in case no instrumental errors are involved, the so obtained difference values using the well-stablished M3C2 algorithm (Lague et al., 2013) have a mean value of 0.01 cm and a standard deviation of about 4 cm. We established a theorical detection threshold of 8 cm (Fig. 4c) that corresponds to two-times the standard deviation of the population with a 95 % of confidence interval, assuming a normal distribution and in accordance with previous research (Abellán et al., 2009). However, in order to visualize the deformation in Fig. 5, we have used a threshold of only 3 cm, which is lower than the theoretical value calculated following the methodology of Abellán et al. (2009). The use of this value, even though it highlights incorrect deformation clusters, allows us to identify the precursor deformation of a rockfall that would not be so clearly visible with an 8 cm treshold.

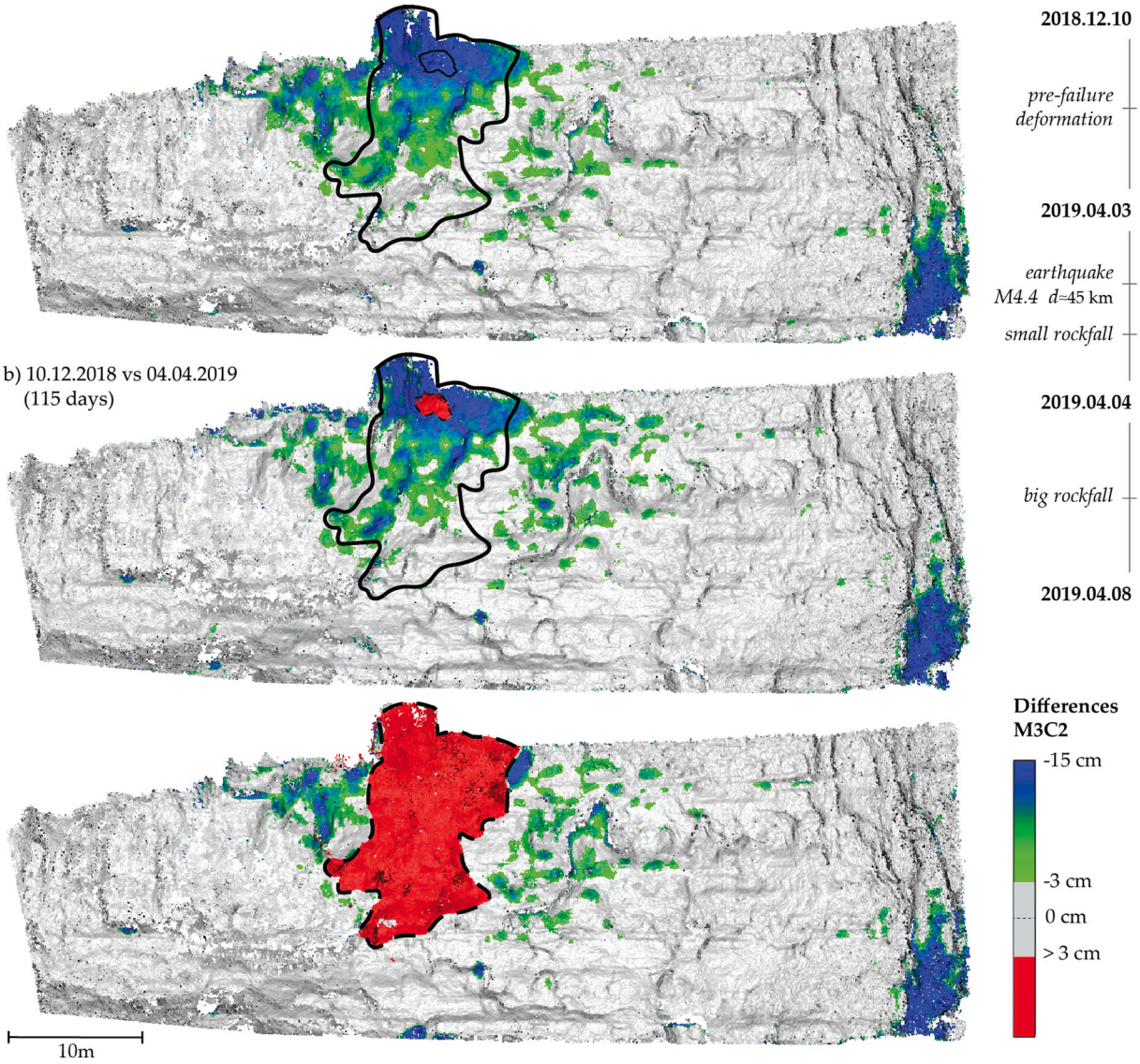


**Fig. 5.** Application example a) Accumulated pre-failure deformation of the active block after 5 months. The comparison has been done with the M3C2 algorithm and the MEMI workflow. b) Comparison performed the day after the earthquake. In red the median rockfall detected before the big one. c) Comparison performed 4/5 days after the earthquake. In red the big rockfall detected. For all images 3 cm has been used as a threshold to maximize the cluster of pre-failure deformation. Noise corresponding to positive values (> 3 cm) have been filtered out keeping only the indicated detachments. On the left, illustrative timeline. (For interpretation of the references to colour in this figure legend, the reader is referred to the web version of this article.)

### 3.2. Power consumption

Power consumption was managed for various Raspberry Pi models, including Zero W, 3B and Pi 4B both in "simplified" and "complex" system configurations. The simplified system involved only the acquisition and storage of images on external USB memory, while the complex system included the additional remote image transmission. The power consumption was analysed in terms of the voltage of the power supply and the efficiency of its conversion to 5 V using 3.7 V (1SxP) and 7.4 V (2SxP) cells. An efficiency of 93 % was obtained when increasing the voltage from the 3.7 V cells to 5 V externally using a DC-DC step. The voltage reduction from the 7.4 V cells was done directly on the WittyPi board with a maximum efficiency of 86 % (UUGear, 2021). It should be noted that the obtained values are a relative estimation between the different configurations, as the real energy consumption is affected by air temperature, current voltage, and battery health.

In addition, a comparison has also been made between the WittyPi 4, with a DC-DC conversion efficiency close to 90 %, and the WittyPi 4 L3V7 that allows the direct powering of the system with 3.7 V cells as it increases the voltage to 5 V internally with an efficiency close to 98 %. Both systems have been run under the simplified version of the code and under stress conditions, acquiring 3 images every 20 min, to test the battery life. The system composed of the 3.7 V – 2800 mAh battery (1S2P) was activated 581 times before it reached a voltage below the standard 3.1 V cut-off voltage, obtaining 1743 images. On the other hand, the 7.4 V – 1400 mAh battery (2S1P) system was started 548 times, capturing 1644 images before the voltage dropped below 6 V. Fig. S4a show the battery life plot for the 1S2P System, and Fig. S4b the battery life plot for the 2S1P configuration.

### 3.3. Contribution to process understanding: Detecting rockfalls and pre-failure deformation

Results in Fig. 5 demonstrate that the proposed very low-cost photogrammetric system can still be used for change detection and real-time monitoring as in previous studies (Abellán et al., 2009; Royán et al., 2014), despite a relative low quality of the input images. This figure shows point cloud differences that were compared using the well-established M3C2 algorithm (Lague et al., 2013). Original point clouds were generated using the advanced MEMI workflow described in Blanch et al. (2021). The colour scale on the image was cut-out on threshold of 3 cm for point cloud comparison both for pre-failure deformation and for rockfall detection to facilitate visual inspection.

Fig. 5a shows the deformation accumulated for 5 months (from 10 December 2018 to 3 April 2019) on a large block that is located in the central part of the cliff. The so calculated deformation in this part of the figure shows a progressive failure characterized by an increase of the deformation values along the vertical, that is reflecting a typical pattern of rock toppling process, i.e., a progressive rotation of a detached block along a horizontal axe (Hungr et al., 2014). It is interesting to note that the deformation displayed in Figs. 5a appeared in advance over the region were the unstable block displayed in Fig. 5c was released after a certain period, meaning that the system could be used for detecting pre-failure deformation in advance on those areas of the cliff experiencing a progressive failure. Moreover, during these 5 months no rockfalls have been detected in the area where the unstable block was located.

On the 3rd of April 2019 an earthquake of magnitude 4.4 occurred with an epicentre 45 km from the cliff, and we hypothesize that this horizontal acceleration was a significant contributing factor in the rockfall episodes displayed in Fig. 5. Fig. 5a shows the point cloud comparison between a stable reference and the model generated with images acquired one hour before the earthquake, which show no signs of rockfall episodes. Fig. 5b shows the results of point cloud comparison using images that were acquired 23 h after the event, displaying a rockfall (approximately 1m$^3$) that occurred in the upper zone of the active block. Eventually, four to five days after the earthquake a larger rockfall at the active block was triggered, which becomes visible in the data from 8th of April 2019 (Fig. 5c). This rockfall has a volume of about 107 m$^3$, and the average deformation between the two models (depth of the rockfall) is 0.82 m. The comparisons of the day after the earthquake (4th of April 2019) and 4 days later (8th of April 2019) were possible thanks to the high temporal frequency of the observations and the remote sending of images. Fig. S5 in the supplementary material shows in detail the rockfall that occurred after the earthquake on 3 April.

## 4. Discussion

### 4.1. Overall approach

The results obtained in rockfall monitoring in Puigcerós, Spain, show that the photogrammetric system presented in this publication are useful in the field of geoscience monitoring based on near-continuous change detection at very low cost. Our very low-cost system represents a balance between image quality, acquisition cost and ease of set-up with simplicity of operation and maintenance, it is shown to be effective for geomorphological monitoring (Santise et al., 2017; Taylor et al., 2023).

More powerful camera monitoring systems capable of higher quality images could also be used (e.g., Kromer et al., 2019; Brezzi et al., 2020; Giacomini et al., 2020; Blanch et al., 2023). However, the acquisition costs, complexity of installation and maintenance are significantly higher, making the instruments less suitable for long-term unattended measurements (Wilkinson et al., 2021). In addition, our system has been built using universal components, all of which are commercially available (no in-house printed circuit boards have been used), which facilitates system expansion and acts as a proof of concept.

The low cost of the change detection monitoring system introduced allows greater exposure of the installation and, therefore, its installation in areas closer to the location of the geohazard. The loss of one of these systems does not have as profound an impact as the loss of instruments such as LiDAR or high-resolution cameras. In addition, very low-cost systems also have other potential advantages, such as being able to develop research in economically limited environments or to perform more sophisticated research for the same cost (e.g., move from a 2D DSLR system to a very low-cost 3D array). A limiting element of our setup is the lack of synchronisation between the systems due to the sequential booting of each device. The delay between captures depends on the drift of each RTC (DS3231SN for WittyPi3) if the WittyPi cannot synchronize the time with the Internet, and on the speed differences between the processors of each device. However, our experience shows that the synchronisation errors are not relevant, especially in the case of change detection for geomorphological monitoring purposes since the differences between images never exceeded a few seconds.

Another limitation of the photogrammetric system identified was the metal boxes. The boxes used have withstood more than two years in a harsh climatic environment, confirming their robustness, durability and watertightness. However, the use of metal housings makes wireless connections difficult due to the Faraday cage effect, which impedes the Wi-Fi signal. An effective way to overcome this limitation is to use wired connections or plastic boxes (UV-resistant) that are permeable in terms of electronic waves (e.g., Santise et al., 2017; Wilkinson et al., 2021) or add an external Wi-Fi antenna outside the box. Thus, the devices we initially installed in Puigcercós had to be adapted to include an external USB Wi-Fi antenna (Fig. 6a).

### 4.2. Hardware and software

Components of commercial hardware can easily be replaced or upgraded with alternatives. For example, microcomputers can be replaced with smaller and cheaper versions, such as the Raspberry Pi Zero W. The camera can also be upgraded with more powerful products, such as the Raspberry Pi Camera HQ with a 12-megapixel sensor and corresponding C-mount lens (Taylor et al., 2023). The use of this sensor

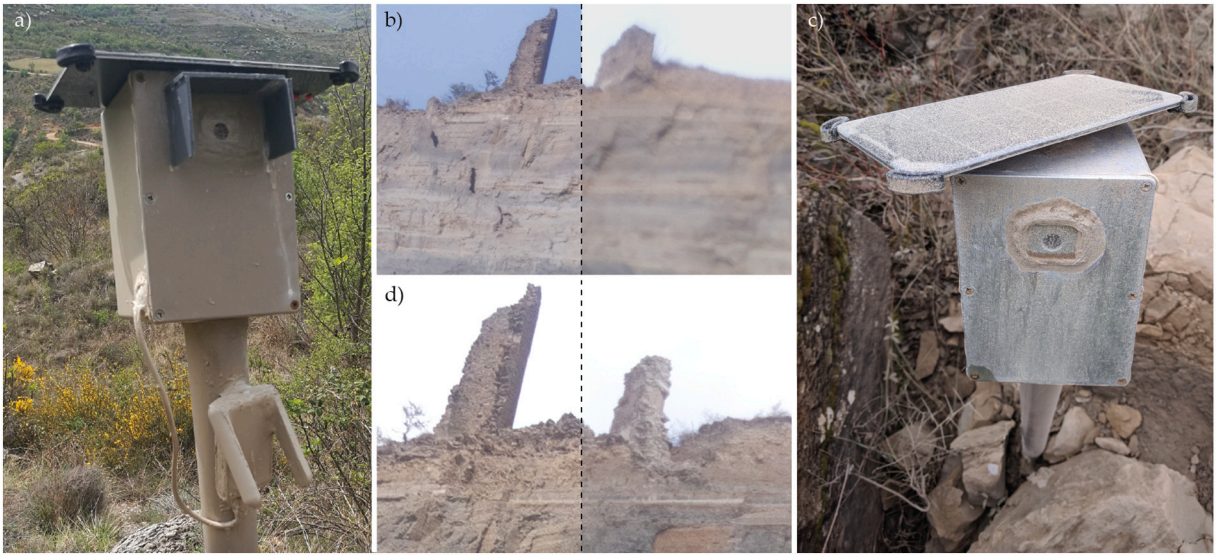


**Fig. 6.** Limitations of the very low-cost system: a) Installation of an external Wi-Fi antenna to overcome the problems related to the Faraday cage effect caused by the metal box. b) Water penetration. Left: image with good sharpness (reference). Right: image affected by water infiltration and fogging of the lab glass. c) System affected by dust caused by a large rockfall. d) Focus differences. Left: image with good sharpness captured on 06/08/2019. Right image with a slight out-of-focus captured on 07/08/2019.

and lens assembly would provide higher quality images but will significantly increase costs compared to the V2 camera that includes the lens (Pi Camera HQ with 6 mm lens, approx. 90€. vs Pi Camera V2, approx. 25€). Nevertheless, the ability to choose the appropriate lens with a specific focal length gives more flexibility and increases the installation possibilities of the system. Furthermore, improving the camera would overcome one of the main limitations of the V2 camera, which is the difficulty in maintaining a stable focus as well as in obtaining reliable internal parameters (i.e., camera calibration; Elias et al., 2020).

To perform the RTC and scheduling tasks, the WittyPi Mini can be used, further reducing installation costs while providing the main functions needed to run the systems. Finally, the energy system can be sized according to the needs of each site. In our case, a 3.5 W solar panel was sufficient to charge the 4000 mAh power bank. Thereby, it should be noted that the location of the cameras is in an open field in Spain (solar radiation of 4.6 kWh/m$^2$day), with panels facing the sun and with a sky view of >140°. The power consumption of the system is highly dependent on its configuration (e.g., number of pictures captured, or time elapsed for sending images). Nevertheless, the system can run for several months on a single battery charge (without solar panel). Other environmental factors such as humidity and temperature can affect power consumption and battery life. The data transmission and image sending steps are the most energy consuming as they consume more resources and increase the system's operating time by approximately two times.

Choosing lithium cells allows for more control over power management, requires less space and is generally less expensive than power bank systems. However, the loss of the plug-and-play option makes it less suitable for rapid integration or for inexperienced users. If solar panels are used to charge, the 7.4 V system, a charger that balances the voltage for each cell is needed. Furthermore, DC-DC converters or chargers with some LED indicators should be avoided because, although they may have very good efficiencies, the consumption may be relevant for long-term monitoring. However, both the results in Table 1 and Fig. S3 show that it is better to work with lower voltage and higher current configurations (e.g., 1S2P: 3.7 V - 2800 mAh) than the same batteries but in 2S1P configuration (7.4 V – 1400 mAh).

The "light" system, configured to capture images and store them only on the USB device, allows very long autonomies with very small batteries and without any solar recharging. It is estimated that the autonomy can exceed nine months with a single 3.7 V cell and 1.400 mAh. However, when it comes to long-term autonomy, the losses and efficiency of the battery itself must be considered. The "complete" system, with remote sending of images, exhibits a reduced battery life.

**Table 1**
Comparison of operational duration and consumed energy for various photogrammetric systems with different Raspberry pi models in a simple script designed to acquire a burst of 5 images. The cycle duration serves as a reference, as it is influenced by various factors including camera shutter speed, writing speed of the microSD or USB drive, and the network speed for transmitting images.

| Limited version (light code) | | | | | |
|---|---|---|---|---|---|
| | Duration | 3.7 V (1SxP) | | 7.4 V (2SxP) | |
| RPi Zero W | 1 m 17 s | 6.6 mAh | 27.0 mWh | 3.9 mAh | 32,3 mWh |
| RPi 3 Model B+ | 40.5 s | 7.4 mAh | 31.0 mWh | 4.5 mAh | 36.3 mWh |
| RPi 4 Model B | 45.1 s | 10.1 mAh | 42.9 mWh | 6.2 mAh | 50.0 mWh |
| Full version (Remote sending) | | | | | |
| | Duration | 3.7 V (1SxP) | | 7.4 V (2SxP) | |
| RPi Zero W | 1 m 42 s | 9.2 mAh | 37.5 mWh | 5.5 mAh | 44,8 mWh |
| RPi 3 Model B+ | 1 m 08 s | 13.0 mAh | 52.9 mWh | 7.6 mAh | 61.7 mWh |
| RPi 4 Model B | 1 m 10s | 16.6 mAh | 66.7 mWh | 9.5 mAh | 77.5 mWh |

### 4.3. Applications in real scenarios

The photogrammetric system developed was successfully installed in a geohazard area and, although the system required no maintenance, it suffered from difficulties. The main problems experienced were climate-related. For example, the glass covering the lens aperture became water permeable after a year, allowing moisture to enter the system. In addition, the high ambient humidity and wide temperature range caused moisture in the housing to condense into water, fogging the glass and affecting image sharpness. (Fig. 6b). Nevertheless, these challenges have proven to be less severe than those documented in more complex systems, such as Blanch et al. (2023), where larger enclosures and lenses have compromised sealing.

In addition, images were sometimes unusable due to the accumulation of dust on the equipment, particularly during periods when rockfalls had occurred, causing dust clouds (Fig. 6c). Images taken on rainy or foggy days and during severe weather such as storms and snowfalls

also had to be discarded (approximately 20 % of the images acquired). Another issue was defocused images due to a weak attachment between the lens and the sensor of the Raspberry Pi Camera Module v2, particularly in extreme weather conditions with significant thermal fluctuations (Fig. 6d). This rendered the images unusable until the camera module was replaced. Regardless of climatic conditions, in this aspect the reliability results are worse compared to the experience in Blanch et al. (2023), where the use of lenses where the focus can be fixed eliminates the possibility of having out-of-focus images.

Taylor et al. (2023), show that displacements of ice over ~1 m in size can be identified with confidence using a Raspberry Pi High Quality camera located at a distance of up to 1.5 km from the glacier front and using only 10 images. Our results show (Figs. 4 and 5) that centimetric displacements can be detected, using even a lower resolution camera (Raspberry Pi Camera V2) in a shorter distance from the object (60 m) and capturing images only from five different positions. Our setup achieved change-detection accuracies (4 cm) that are coherent with results shown by Blanch et al. (2020) and are comparable to older studies at the same site using LiDAR point clouds (i.e., accuracies of 1.68 cm in Abellán et al. (2009)).

However, it should be noted that this standard deviation is influenced by the parameters used in the M3C2 algorithm. In addition, the entire cliff has been used to obtain the error value, including the most peripheral areas where the photogrammetric models reveal a lower reconstruction quality. Therefore, worse accuracies are to be expected. For example, in Fig. 5 there is a deformation in the lower right margin of the cliff, and it is uncertain whether this is a true pre-fault deformation or an artefact of the reconstruction.

Although the standard deviation gives an indication of the error, in practical monitoring cases, detection thresholds below this value might be chosen, because other properties such as error distribution and point density are relevant, as well. As an example, we used a deformation threshold of 3 cm because, given the distribution of errors, it was sufficient to identify both pre-failure deformation and rockfalls in the main area of the cliff.

Finally, our rockfall monitoring system highlights the advantages of a highly cost-effective fixed monitoring system, capable of capturing data at a remarkably high temporal frequency. This not only allows us to correlate rockfall events with other phenomena, such as rainfall (Blanch et al., 2023), and other environmental factors but also ensures that smaller events occurring before a rockfall are accurately identified in terms of both their number and volume.

Beyond its immediate application to rockfall monitoring, our system and the accompanying codes offer extensive opportunities in a range of geoscientific fields that benefit from change detection monitoring. For instance, in glaciology, real-time monitoring could significantly enhance our understanding of ice dynamics (Taylor et al., 2023). Additionally, in the context of other natural hazards like landslides, early detection of ground movements could greatly improve risk evaluations. Moreover, the capabilities of real-time data transmission, as detailed in our methods, open up exciting possibilities for advanced monitoring and hazard detection, drawing us closer to low-cost early warning systems based on nearly continuous change measurements.

The integration of near-real-time and high-frequency observations brings us closer to accessible and scalable real-time 4D monitoring in the geomorphological sciences. This will be a significant step forward as we will be able to better understand the processes of change, anticipate the risks associated with ongoing phenomena and take proactive measures to mitigate them. This advancement not only allows resource-rich communities to explore a wider range of areas of interest but also empowers financially challenged communities by overcoming the access barriers posed by conventional monitoring methods like LiDAR. In both scenarios, there is an increase in the volume of data collected, and a broadening of the regions under observation, resulting in a more comprehensive understanding of our environment and its mechanisms, and consequently leading to improved mitigation tactics for safeguarding society from natural threats.

## 5. Conclusions

The presented very low-cost photogrammetric monitoring system has been successfully designed and implemented. The open-source codes supporting the system, as well as the guidelines provided for system assembly, allow the creation of photogrammetric systems that can be operated for long periods of time. The installation of five camera units allowed daily monitoring of rockfall activity. The image quality of the system was sufficient to produce 3D models for change detection. The frequency of data acquisition allows near real-time monitoring in 3D, which is difficult to achieve with other monitoring strategies on a limited budget.

Although the level of detection in change detection analysis achieved do not exceed those obtained with more expensive monitoring systems, the flexibility and ease of installation of the equipment and the ability of the systems to collect data periodically and transmit it remotely allow near real-time monitoring, an advantage which, together with the low cost, more than compensates for the disadvantages. The results obtained show that very low-cost photogrammetric systems (especially fixed installations) are effective for geohazard monitoring.

Code availability.

All the necessary codes supporting the contents of this publication are available in the first author digital repository: https://github.com/xabierblanch/RasPi-System.

## Author contributions

XB: Conceptualization, methodology, software, investigation, writing-original, figures; MG: conceptualization, writing - review and editing, supervision; AE: conceptualization, methodology, writing - review and editing, supervision; AA: conceptualization, writing - review and editing, supervision.

## Disclaimer

All data, figures and codes provided in this publication are published under open-source license. The content of this publication is adapted from the Doctoral Thesis of the first author (Blanch, 2022), that is available at the following link: http://hdl.handle.net/2445/189157

## Financial support

The presented study was supported by the PROMONTEC Project (CGL2017-84720-R) funded by the Ministry of Science, Innovation and Universities (MICINN-FEDER). The first author (X. Blanch) was supported by an APIF grant funded by the University of Barcelona. Anette Eltner was funded by the DFG (EL 926/3-1).

## CRediT authorship contribution statement

**Xabier Blanch:** Writing – original draft, Visualization, Software, Methodology, Investigation, Conceptualization. **Marta Guinau:** Writing – review & editing, Supervision, Conceptualization. **Anette Eltner:** Writing – review & editing, Supervision, Methodology, Conceptualization. **Antonio Abellan:** Writing – review & editing, Supervision, Conceptualization.

## Declaration of competing interest

The authors declare that they have no known competing financial interests or personal relationships that could have appeared to influence the work reported in this paper.

The use of brand names in the manuscript has been made without any commercial relationship and for the exclusive purpose of ensuring

the replicability of the systems.

## Data availability

Data will be made available on request.

## Acknowledgments

The authors would like to thank Origens UNESCO Global Geopark for granting permission to work on the Puigcercós cliff, the doctoral thesis examining board for their comments that have improved this publication, and the reviewers and editor for their valuable comments and suggestions that helped to improve this manuscript.

## Appendix A

Very low-cost 3D photogrammetric model (Puigcercós cliff, Spain): https://skfb.ly/o7Qx6.

## Appendix B

Raspbian + WittyPi image for Raspberry Pi camera system (1.0.1): https://zenodo.org/records/7985041.

## Appendix C. Supplementary data

Supplementary data to this article can be found online at https://doi.org/10.1016/j.geomorph.2024.109065.

## References

Abellán, A., Jaboyedoff, M., Oppikofer, T., Vilaplana, J.M., 2009. Detection of millimetric deformation using a terrestrial laser scanner: Experiment and application to a rockfall event. Nat. Hazards Earth Syst. Sci. 9, 365–372. https://doi.org/10.5194/nhess-9-365-2009.

Anderson, K., Westoby, M.J., James, M.R., 2019. Low-budget topographic surveying comes of age: Structure from motion photogrammetry in geography and the geosciences. Prog. Phys. Geogr.: Earth Environ. 43, 163–173. https://doi.org/10.1177/0309133319837454.

Blanch, X., 2022. Developing Advanced Photogrammetric Methods for Automated Rockfall Monitoring. Doctoral dissertation. Universitat de Barcelona. Retrieved from: http://hdl.handle.net/10803/675397.

Blanch, X., Abellan, A., Guinau, M., 2020. Point Cloud Stacking: a Workflow to Enhance 3D monitoring Capabilities using Time-Lapse Cameras. Remote Sens. (Basel) 12, 1240. https://doi.org/10.3390/rs12081240.

Blanch, X., Eltner, A., Guinau, M., Abellan, A., 2021. Multi-Epoch and Multi-Imagery (MEMI) Photogrammetric Workflow for Enhanced Change Detection using Time-Lapse Cameras. Remote Sens. (Basel) 13, 1460. https://doi.org/10.3390/rs13081460.

Blanch, X., Guinau, M., Eltner, A., Abellan, A., 2023. Fixed photogrammetric systems for natural hazard monitoring with high spatio-temporal resolution. Nat. Hazards Earth Syst. Sci. 23, 3285–3303. https://doi.org/10.5194/nhess-23-3285-2023.

Bowman, R., Vodenicharski, B., Collins, J., Stirling, J., 2019. Flat-field and colour correction for the Raspberry Pi camera module. J. Open Hardware 4 (1), 1. https://doi.org/10.5334/joh.20.

Brezzi, L., Gabrieli, F., Cola, S., Lorenzetti, G., Spiezia, N., Bisson, A., Allegrini, M., 2020. Digital terrestrial stereo-photogrammetry for monitoring landslide displacements: a case study in Recoaro Terme (VI). Lecture Notes in Civil Engineering. 155–163. https://doi.org/10.1007/978-3-030-21359-6_17.

Colomina, I., Molina, P., 2014. Unmanned aerial systems for photogrammetry and remote sensing: a review. ISPRS J. Photogramm. Remote Sens. 92, 79–97. https://doi.org/10.1016/J.ISPRSJPRS.2014.02.013.

Elias, M., Eltner, A., Liebold, F., Maas, H.G., 2020. Assessing the influence of temperature changes on the geometric stability of smartphone- and raspberry pi cameras. Sensors 2020 20, 643. https://doi.org/10.3390/S20030643. Page 643 20.

Eltner, A., Sofia, G., 2020. Structure from motion photogrammetric technique. Developments in Earth Surface Processes. 1–24. https://doi.org/10.1016/B978-0-444-64177-9.00001-1.

Eltner, A., Kaiser, A., Castillo, C., Rock, G., Neugirg, F., Abellán, A., 2016. Image-based surface reconstruction in geomorphometry-merits, limits and developments. Earth Surf. Dyn. 4, 359–389. https://doi.org/10.5194/esurf-4-359-2016.

Eltner, A., Kaiser, A., Abellan, A., Schindewolf, M., 2017. Time lapse structure-from-motion photogrammetry for continuous geomorphic monitoring. Earth Surf. Process. Landf. 42, 2240–2253. https://doi.org/10.1002/esp.4178.

Eltner, A., Elias, M., Sardemann, H., Spieler, D., 2018. Automatic image-based water stage measurement for long-term observations in ungauged catchments. Water Resour. Res. 54, 10,362–10,371. https://doi.org/10.1029/2018WR023913.

Eltner, A., Bressan, P.O., Akiyama, T., Gonçalves, W.N., Marcato Junior, J., 2021. Using Deep Learning for Automatic Water Stage Measurements. Water Resour. Res. 57 https://doi.org/10.1029/2020WR027608.

Feurer, D., Vinatier, F., 2018. Joining multi-epoch archival aerial images in a single SfM block allows 3-D change detection with almost exclusively image information. ISPRS J. Photogramm. Remote Sens. 146, 495–506. https://doi.org/10.1016/j.isprsjprs.2018.10.016.

Giacomini, A., Thoeni, K., Santise, M., Diotri, F., Booth, S., Fityus, S., Roncella, R., 2020. Temporal-Spatial Frequency Rockfall Data from Open-pit Highwalls using a Low-cost monitoring System. Remote Sens. (Basel) 12, 2459. https://doi.org/10.3390/rs12152459.

Giordan, D., Luzi, G., Monserrat, O., Dematteis, N., 2022. Remote Sensing Analysis of Geologic Hazards. Remote Sens. (Basel) 14, 4818. https://doi.org/10.3390/rs14194818.

Gonçalves, J.A., Henriques, R., 2015. UAV photogrammetry for topographic monitoring of coastal areas. ISPRS J. Photogramm. Remote Sens. 104, 101–111. https://doi.org/10.1016/J.ISPRSJPRS.2015.02.009.

Hungr, O., Leroueil, S., Picarelli, L., 2014. The Varnes classification of landslide types, an update. Landslides 11, 167–194. https://doi.org/10.1007/s10346-013-0436-y.

Iglhaut, J., Cabo, C., Puliti, S., Piermattei, L., O'Connor, J., Rosette, J., 2019. Structure from Motion Photogrammetry in Forestry: A Review. For. Rep, Curr. https://doi.org/10.1007/s40725-019-00094-3.

James, M.R., Robson, S., 2014. Mitigating systematic error in topographic models derived from UAV and ground-based image networks. Earth Surf. Process. Landf. 39, 1413–1420. https://doi.org/10.1002/esp.3609.

Jin, D., Li, J., Gong, J., Li, Yi, Zhao, Z., Li, Yongzhi, Li, D., Yu, K., Wang, S., 2021. Shipborne mobile photogrammetry for 3D mapping and landslide detection of the water-level fluctuation zone in the Three Gorges Reservoir Area, China. Remote Sens. (Basel) 13, 1007. https://doi.org/10.3390/RS13051007. Page 1007 13.

Jolles, J.W., 2021. Broad-scale applications of the Raspberry Pi: a review and guide for biologists. Methods Ecol. Evol. 12, 1562–1579. https://doi.org/10.1111/2041-210X.13652.

Kaiser, A., Neugirg, F., Rock, G., Müller, C., Haas, F., Ries, J., Schmidt, J., 2014. Small-scale surface reconstruction and volume calculation of soil erosion in complex moroccan Gully morphology using structure from motion. Remote Sens. (Basel) 6, 7050–7080. https://doi.org/10.3390/rs6087050.

Kishan, H., Vappangi, S., Bandi, D., Subramanian, M., Ellison Mathe, S., 2022. A review of image processing applications based on Raspberry-Pi; a review of image processing applications based on Raspberry-Pi. In: 8th International Conference on Advanced Computing and Communication Systems (ICACCS) 1. https://doi.org/10.1109/ICACCS54159.2022.9784958.

Kromer, R., Walton, G., Gray, B., Lato, M., Group, R, 2019. Development and optimization of an automated fixed-location time lapse photogrammetric rock slope monitoring system. Remote Sens. (Basel) 11, 1890. https://doi.org/10.3390/rs11161890.

Lague, D., Brodu, N., Leroux, J., 2013. Accurate 3D comparison of complex topography with terrestrial laser scanner: Application to the Rangitikei canyon (N-Z). ISPRS J. Photogramm. Remote Sens. 82, 10–26. https://doi.org/10.1016/j.isprsjprs.2013.04.009.

Leprince, S., Berthier, E., Ayoub, F., Delacourt, C., Avouac, J.-P., 2008. Monitoring Earth surface dynamics with optical imagery. Eos. Trans. AGU 89 (1), 1–2. https://doi.org/10.1029/2008EO010001.

Luhmann, T., Fraser, C., Maas, H.G., 2016. Sensor modelling and camera calibration for close-range photogrammetry. ISPRS J. Photogramm. Remote Sens. 115, 37–46. https://doi.org/10.1016/j.isprsjprs.2015.10.006.

Minowa, M., Podolskiy, E.A., Sugiyama, S., Sakakibara, D., Skvarca, P., 2018. Glacier calving observed with time-lapse imagery and tsunami waves at Glaciar Perito Moreno, Patagonia. J. Glaciol. 64, 362–376. https://doi.org/10.1017/JOG.2018.28.

Neugirg, F., Stark, M., Kaiser, A., Vlacilova, M., della Seta, M., Vergari, F., Schmidt, J., Becht, M., Haas, F., 2016. Erosion processes in calanchi in the Upper Orcia Valley, Southern Tuscany, Italy based on multitemporal high-resolution terrestrial LiDAR and UAV surveys. Geomorphology 269, 8–22. https://doi.org/10.1016/j.geomorph.2016.06.027.

Pagnutti, M.A., Ryan, R., Cazenavette, V., Gold, M.J., Harlan, R., Leggett, E., Pagnutti, J. F., 2017. Laying the foundation to use Raspberry Pi 3 V2 camera module imagery for scientific and engineering purposes. J. Electron. Imag. 26 (1) https://doi.org/10.1117/1.JEI.26.1.013014.

Patrick, M.R., Orr, T., Antolik, L., Lee, L., Kamibayashi, K., 2014. Continuous monitoring of Hawaiian volcanoes with thermal cameras. J. Appl. Volcanol. 3, 1. https://doi.org/10.1186/2191-5040-3-1.

Piras, M., Grasso, N., Abdul Jabbar, A., 2017. UAV Photogrammetric solution using a Raspberry Pi Camera Module and smart devices: Test and results. Int. Arch. Photogramm. Remote Sens. Spatial Inf. Sci. XLII-2/W6, 289–296. https://doi.org/10.5194/isprs-archives-XLII-2-W6-289-2017.

Rivera, A., Corripio, J., Bravo, C., Cisternas, S., 2012. Glaciar Jorge Montt (Chilean Patagonia) dynamics derived from photos obtained by fixed cameras and satellite image feature tracking. Ann. Glaciol. 53, 147–155. https://doi.org/10.3189/2012AoG60A152.

Roncella, R., Forlani, G., Fornari, M., Diotri, F., 2014. Landslide monitoring by fixed-base terrestrial stereo-photogrammetry. ISPRS Ann. Photogramm. Remote Sens. Spatial. Inform. Sci. II–5, 297–304. https://doi.org/10.5194/isprsannals-II-5-297-2014.

Royán, M.J., Abellán, A., Jaboyedoff, M., Vilaplana, J.M., Calvet, J., 2014. Spatio-temporal analysis of rockfall pre-failure deformation using Terrestrial LiDAR. Landslides 11, 697–709. https://doi.org/10.1007/s10346-013-0442-0.

Santise, M., Thoeni, K., Roncella, R., Sloan, S.W., Giacomini, A., 2017. Preliminary tests of a new low-cost photogrammetric system. Int. Arch. Photogramm. Remote Sens.

Spatial Inf. Sci. XLII-2/W8, 229–236. https://doi.org/10.5194/isprs-archives-XLII-2-W8-229-2017.

Scaioni, M., Longoni, L., Melillo, V., Papini, M., 2014. Remote Sensing for Landslide Investigations: an Overview of recent Achievements and Perspectives. Remote Sens. (Basel) 6, 9600–9652. https://doi.org/10.3390/rs6109600.

Spampinato, L., Calvari, S., Oppenheimer, C., Boschi, E., 2011. Volcano surveillance using infrared cameras. Earth Sci. Rev. 106, 63–91. https://doi.org/10.1016/j.earscirev.2011.01.003.

Stöcker, C., Eltner, A., Karrasch, P., 2015. Measuring gullies by synergetic application of UAV and close range photogrammetry — a case study from Andalusia, Spain. Catena (Amst) 132, 1–11. https://doi.org/10.1016/j.catena.2015.04.004.

Taylor, L.S., Quincey, D.J., Smith, M.W., Baumhoer, C.A., McMillan, M., Mansell, D.T., 2021. Remote sensing of the mountain cryosphere: current capabilities and future opportunities for research. Prog. Phys. Geogr.: Earth Environ. 45, 931–964. https://doi.org/10.1177/03091333211023690.

Taylor, L.S., Quincey, D.J., Smith, M.W., 2023. Evaluation of low-cost Raspberry Pi sensors for structure-from-motion reconstructions of glacier calving fronts. Nat. Hazards Earth Syst. Sci. 23, 329–341. https://doi.org/10.5194/nhess-23-329-2023.

Toth, C., Jóźków, G., 2016. Remote sensing platforms and sensors: a survey. ISPRS J. Photogramm. Remote Sens. 115, 22–36. https://doi.org/10.1016/j.isprsjprs.2015.10.004.

UUGear, 2021. WittyPi3 - User Manual (revision 1.06). http://www.uugear.com/doc/WittyPi3_UserManual.pdf.

Vedavalli, P., Kondaveeti, H.K., Deepak, C.H., 2022. A Review on Automated monitoring applications of Raspberry Pi. 8th International Conference on Advanced Computing and Communication Systems. ICACCS 2022, 485–492. https://doi.org/10.1109/ICACCS54159.2022.9785271.

Westoby, M.J., Brasington, J., Glasser, N.F., Hambrey, M.J., Reynolds, J.M., 2012. 'Structure-from-Motion' photogrammetry: a low-cost, effective tool for geoscience applications. Geomorphology 179, 300–314. https://doi.org/10.1016/j.geomorph.2012.08.021.

Wilkinson, M., Bell, M.C., Morison, J.I.L., Alberto Silva, C., 2021. A Raspberry Pi-based camera system and image processing procedure for low cost and long-term monitoring of forest canopy dynamics. Methods Ecol. Evol. 12, 1316–1322. https://doi.org/10.1111/2041-210X.13610.